ATP7A and ATP7B copper transporters have distinct functions in the regulation of neuronal dopamine-β-hydroxylase

Received for publication, July 13, 2018, and in revised form, October 17, 2018 Published, Papers in Press, October 19, 2018, DOI 10.1074/jbc.RA118.004889

Katharina Schmidt[‡], Martina Ralle[§], Thomas Schaffer[¶], Samuel Jayakanthan[‡], Bilal Bari[‖], Abigael Muchenditsi[‡], and Svetlana Lutsenko[‡1]

From the [‡]Department of Physiology, Johns Hopkins University School of Medicine, Baltimore, Maryland 21205, the [§]Department of Molecular and Medical Genetics, Oregon Health and Science University, Portland, Oregon 97239, the [¶]Department of Biological Chemistry, Johns Hopkins University, Baltimore, Maryland 21205, and the [‖]Department of Neuroscience, Brain Science Institute, Johns Hopkins University, Baltimore, Maryland 21205

Edited by Ruma Banerjee

The copper (Cu) transporters ATPase copper-transporting alpha (ATP7A) and ATPase copper-transporting beta (ATP7B) are essential for the normal function of the mammalian central nervous system. Inactivation of ATP7A or ATP7B causes the severe neurological disorders, Menkes disease and Wilson disease, respectively. In both diseases, Cu imbalance is associated with abnormal levels of the catecholamine-type neurotransmitters dopamine and norepinephrine. Dopamine is converted to norepinephrine by dopamine-β-hydroxylase (DBH), which acquires its essential Cu cofactor from ATP7A. However, the role of ATP7B in catecholamine homeostasis is unclear. Here, using immunostaining of mouse brain sections and cultured cells, we show that DBH-containing neurons express both ATP7A and ATP7B. The two transporters are located in distinct cellular compartments and oppositely regulate the export of soluble DBH from cultured neuronal cells under resting conditions. Down-regulation of ATP7A, overexpression of ATP7B, and pharmacological Cu depletion increased DBH retention in cells. In contrast, ATP7B inactivation elevated extracellular DBH. Proteolytic processing and the specific activity of exported DBH were not affected by changes in ATP7B levels. These results establish distinct regulatory roles for ATP7A and ATP7B in neuronal cells and explain, in part, the lack of functional compensation between these two transporters in human disorders of Cu imbalance.

Copper (Cu) homeostasis is essential for the normal development and function of the mammalian brain (1–8). Either Cu deficiency or excess is highly detrimental. Two ATP-driven Cu transporters, ATP7A and ATP7B, play essential roles in balancing Cu levels in the brain. Inactivating mutations in either ATP7A or ATP7B are associated with severe neurologic disorders (Menkes disease and Wilson disease, respectively). In Menkes disease, one of the major biochemical hallmarks is an increased ratio of dopamine (DA)[2] to norepinephrine (NE), which is used as an early diagnostic marker of this disorder (9–12). In Wilson disease, catecholamine metabolism is also altered, as evidenced by a diminished secretion of DA and NE as well as an abnormal functioning of the dopaminergic system (13). Wilson disease patients present with parkinsonism, psychotic episodes, and schizophrenia, in addition to a spectrum of neurologic abnormalities. These clinical observations and similar findings in animal models of the Cu-related disorders suggest that both ATP7A and ATP7B contribute to catecholamine metabolism in the brain. However, our knowledge about specific roles of these transporters is very limited.

Dopamine-β-hydroxylase (DBH) is an important molecular link between the catecholamine metabolism and neuronal Cu homeostasis. This essential enzyme converts DA to NE in a reaction that requires a bound Cu cofactor (14, 15). DBH obtains Cu within the lumen of the secretory pathway during its biosynthetic maturation. Current evidence suggests that ATP7A, which transfers Cu from the cytosol into the lumen of the *trans*-Golgi network (TGN), is a likely supplier of Cu for DBH (16). Patients with Menkes disease and animals with inactive ATP7A have lower DBH activity, as indicated by an increased DA/NE ratio (9–12). The adrenal gland (another site with high DBH levels) expresses only ATP7A (17, 18); therefore, ATP7A is sufficient for DBH activation, at least in the adrenal tissue. In the brain, both ATP7A and ATP7B are present; however, the role of ATP7B, which is highly homologous to ATP7A, remains unclear. We hypothesized that ATP7B may affect DBH activity indirectly by altering Cu levels in the cytosol or regulating the cellular behavior of DBH. By testing this hypothesis, we discovered a previously unanticipated role for both of the Cu transporters in the regulation of DBH export from neuronal cells.

This work was supported by National Institute of Health Grant 2R01GM101502 (to S. L.). The authors declare that they have no conflicts of interest with the contents of this article. The content is solely the responsibility of the authors and does not necessarily represent the official views of the National Institutes of Health.

[1] To whom correspondence should be addressed. Tel.: 410-614-4661; E-mail: lutsenko@jhmi.edu.

[2] The abbreviations used are: DA, dopamine; NE, norepinephrine; DBH, dopamine–hydroxylase; TGN, trans-Golgi network; LC, locus coeruleus; BCS, bathocuproine disulfonate; CCS, copper chaperone for SOD1; TTM, tetrathiomolybdate; PFA, paraformaldehyde; PBST, Triton-X in PBS; DAPI, 4′,6-diamidino-2-phenylindole; XFM, X-ray fluorescence microscopy; MEM, minimal essential medium; RIPA, radioimmune precipitation assay; CAPS, 3-(cyclohexylamino)propanesulfonic acid.

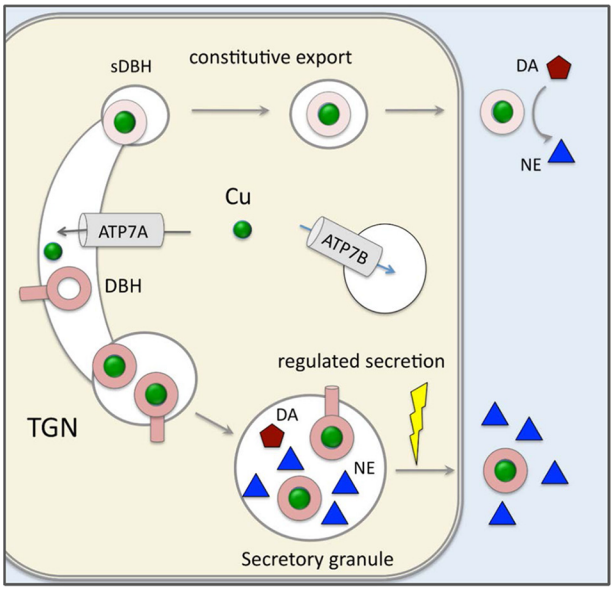

Figure 1. Cartoon illustrating the intracellular distribution of ATP7A, ATP7B, and DBH. ATP7A is located in the TGN and transports copper (*green balls*) into the lumen of this compartment. ATP7B is in vesicles where it sequesters Cu from the cytosol and regulates the amount of cytosolic Cu available to ATP7A. DBH receives its Cu cofactor as it matures within the secretory pathway (most likely from ATP7A). The fraction of DBH is then proteolytically processed. Soluble DBH is sorted to two main destinations. Some soluble DBH and a noncleaved membrane-bound DBH are sorted to secretory granules. In secretory granules, DBH converts DA into NE, which is secreted together with the soluble DBH into the extracellular space in response to extracellular stimuli (*regulated secretion*). Another fraction of soluble DBH is modified within the secretory pathway and sorted to vesicles, which undergo constitutive trafficking to the plasma membrane. The vesicles fuse with the membrane and export active soluble DBH in the absence of neuronal stimulation (*constitutive export*).

DBH exists in three forms, which have different fates within the secretory pathway (Fig. 1). Membrane-bound DBH is targeted to secretory granules. In granules, it converts DA to NE, which is released from cells in response to neuronal activation. Soluble DBH is generated from the membrane-bound DBH through proteolysis, which occurs in the early compartments of the secretory pathway, most likely in the TGN (19, 20). Soluble DBH has two destinations. It is sorted similarly to the membrane-bound DBH into secretory granules and then secreted from cells along with NE in response to neuronal activation (regulated secretion). In addition, soluble DBH is sulfated (21) and then exported from cells under resting conditions (export/constitutive secretion). The fraction of soluble DBH directed for constitutive secretion is relatively minor (7–12% of a newly synthesized DBH (21), with very little known about this process. Available data suggest that the constitutive secretion maintains stable levels of DBH in the cerebrospinal fluid, as these levels are independent of neuronal activity (22). We found that the constitutive secretion of DBH requires Cu and is tightly and oppositely regulated by ATP7A and ATP7B. This unexpected finding brought to light a new functional link between Cu homeostasis and catecholamine balance; thus the results of this study have implication for several neuropsychiatric disorders, in which Cu levels in noradrenergic neurons are altered.

Results

Cu is selectively enriched in mouse locus coeruleus

To better understand the role of copper transporters in regulating DBH, we first characterized the Cu status of the locus coeruleus (LC), the major hub of DBH expressing neurons in the central nervous system (Fig. 2*a*). Previously, the importance of Cu homeostasis in the LC was suggested by its high Cu content in humans (23, 24). To determine whether high Cu in the LC is common for different species, we quantitatively imaged Cu in coronal sections of adult mouse brain using X-ray fluorescence microscopy (Fig. 2). The LC was identified by high DBH expression (Fig. 2*b*). Throughout the entire coronal section, Cu levels were fairly uniform (Fig. 2*c*). The notable exceptions were ventricles, where Cu enters the brain (25), and the LC: both regions had much higher Cu levels compared with the rest of the parenchyma (Fig. 2*d*). In ventricles, several metals were elevated including copper, potassium, and zinc. In the LC, only Cu was elevated (Fig. 2*c*). To account for possible variations in the sections' thickness, we normalized the Cu levels to zinc and found that Cu levels in the LC were three times higher than in the pons (1.01 ± 0.08 *versus* 0.33 ± 0.01 mM) (Fig. 2, *e* and *f*). This significant enrichment of Cu in the LC across species pointed to the importance of Cu homeostasis in LC physiology.

Noradrenergic neurons express ATP7A and ATP7B in distinct intracellular locations

To determine whether ATP7A regulates Cu homeostasis in the LC alone or together with ATP7B, we immunostained mouse brain sections with anti-ATP7A or anti-ATP7B antibodies (Fig. 3). Co-staining with DBH, used as an LC marker, demonstrated that ATP7A was present in mouse LC and was more abundant in this region compared with the surrounding tissue (Fig. 3*a*). Immunostaining of ATP7B also showed expression and similar enrichment of ATP7B in the LC (Fig. 3*b*). The specificity of ATP7B staining was confirmed by the absence of a signal in the LC of the ATP7B$^{-/-}$ brain (Fig. 3*c*). The specificity of ATP7A antibody was verified by the presence in the Western blotting of the band with the expected mass in cells expressing ATP7A and the absence of this band in HepG2 cells (which do not express ATP7A). Within the LC, ATP7A and ATP7B were present in the same neurons, but their intracellular localization was very different. ATP7B was vesicular and distributed throughout the cytosol, whereas ATP7A was perinuclear and clustered at the side of the nucleus (Fig. 3*d*). There was little, if any, overlap between the ATP7A and ATP7B patterns. Thus, both of the Cu transporters contribute to Cu homeostasis in the LC neurons and appear to function in distinct intracellular compartments.

Validating SH-SY5Y cells as a model to study Cu homeostasis and DBH function

Mouse LC is tiny (~0.03 mm^3) and difficult to study biochemically. Consequently, to characterize the role of Cu homeostasis in DBH regulation, we initially used SH-SY5Y cells. These cells express adrenergic markers and can be differentiated to have a neuron-like morphology (26). ATP7A and

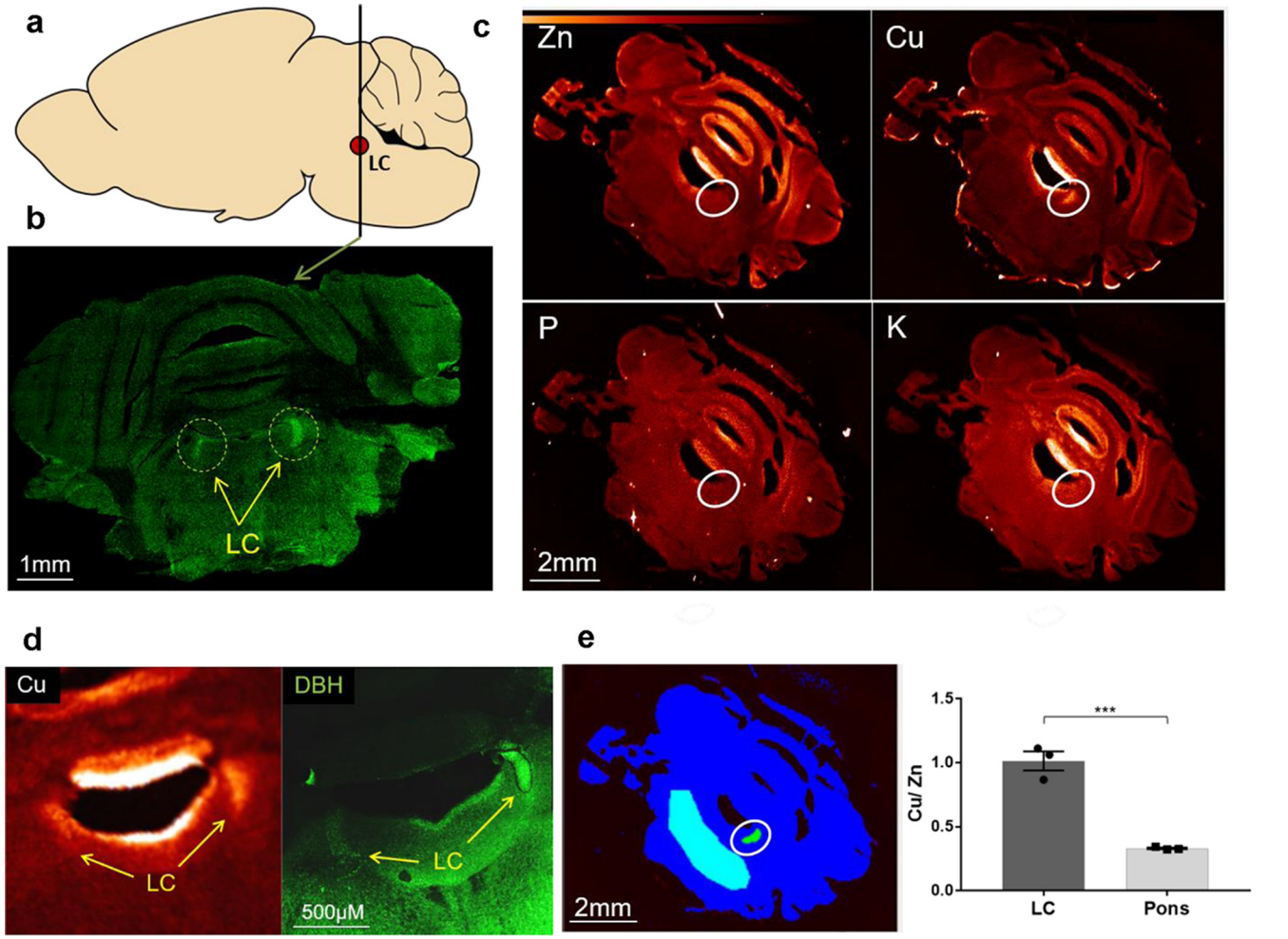

Figure 2. Copper is enriched in the mouse locus coeruleus. *a*, the diagram of a mouse brain (a sagittal view); the line shows the location where coronal sections were taken. The *red dot* represents the LC. *b*, representative tiled confocal image of the coronal section immunostained for DBH. Regions with high expression of DBH indicate LC (*circles*). *c*, XFM images for metals. The map of phosphate, which has stable levels in cells, is used as a control. The enrichment of Cu in the LC region is evident from the *lighter color*. Other metals (potassium (*K*), phosphorus (*P*), and zinc (*Zn*)) were not elevated in the LC and are shown to illustrate the specificity of Cu enrichment. *d*, consecutive brain sections were used to verify that high Cu levels occur in the LC; one section was imaged using XFM and the adjacent section was immunostained for DBH. *Left*, XFM image shows high Cu fluorescence (indicated by a *light color*) in ventricles and in the LC. *Right*, immunostaining of DBH confirms high Cu in the LC. *e*, *left*, a schematic illustrating the areas (in *turquoise*) that were used for comparison of Cu levels: LC (*circled*) and the region outside of LC (the pons). *Right*, Cu/Zn ratio in the LC and pons regions (1.01 ± 0.08 and 0.33 ± 0.01, respectively; $n = 3$; $p = 0.001$).

ATP7B were both expressed in either nondifferentiated or differentiated SH-SY5Y cells (Fig. 4*a*) in agreement with a previous report (27). Similar to the LC, in SH-SY5Y cells ATP7A had a predominantly asymmetric perinuclear pattern (Fig. 4*c*). Co-staining with TGN46 (a marker of the *trans*-Golgi network) demonstrated that ATP7A was targeted primarily to the TGN. A small fraction of ATP7A was detected in vesicles (Fig. 4*c*). The ATP7B pattern was mostly vesicular, and the overlap with TGN46 was minor (Fig. 4*d*). Similar to the LC neurons, there was little overlap between ATP7A and ATP7B in vesicles (Fig. 4*e*). To test whether the co-expression of ATP7A and ATP7B would be observed in other DBH-containing neurons, we examined primary cortical neurons. In these cells, ATP7A and ATP7B were both expressed; ATP7A was found clustered at the axonal side of the nuclei, whereas ATP7B was present in vesicles distributed around the nucleus and in the cytosol (Fig. 4*f*).

Differentiated SH-SY5Y cells have high levels of DBH and produce both the soluble (smaller) DBH and the membrane-bound (larger) DBH (Fig. 4*a*). Typically, two bands (membrane-bound and soluble) are detected on Western blots; occasionally, the lower band appears as a doublet (Fig. 4*b*).

SH-SY5Y cells export soluble DBH under basal (resting) conditions (Fig. 4*b*, *upper panel*). The nonsaturable time-dependent increase in the amount of extracellular DBH (Fig. 4*b*) indicates that the export of soluble DBH significantly exceeded the re-uptake. To measure DBH activity, we analyzed the hydroxylation of the DBH substrate tyramine in the presence and absence of a specific DBH inhibitor, nepicastat. Over 75% of the tyramine hydroxylation was because of DBH activity (Fig. 4*b*, *lower left*). The activity of DBH in the extracellular medium increased with time and positively correlated with the amount of DBH protein (Fig. 4*b*, *lower right*). Thus, similar to LC neurons, SH-SY5Y cells express and secrete active DBH and have relevant Cu transporters to regulate Cu homeostasis. These characteristics make SH-SY5Y cells a useful model for studying the role of Cu in DBH regulation.

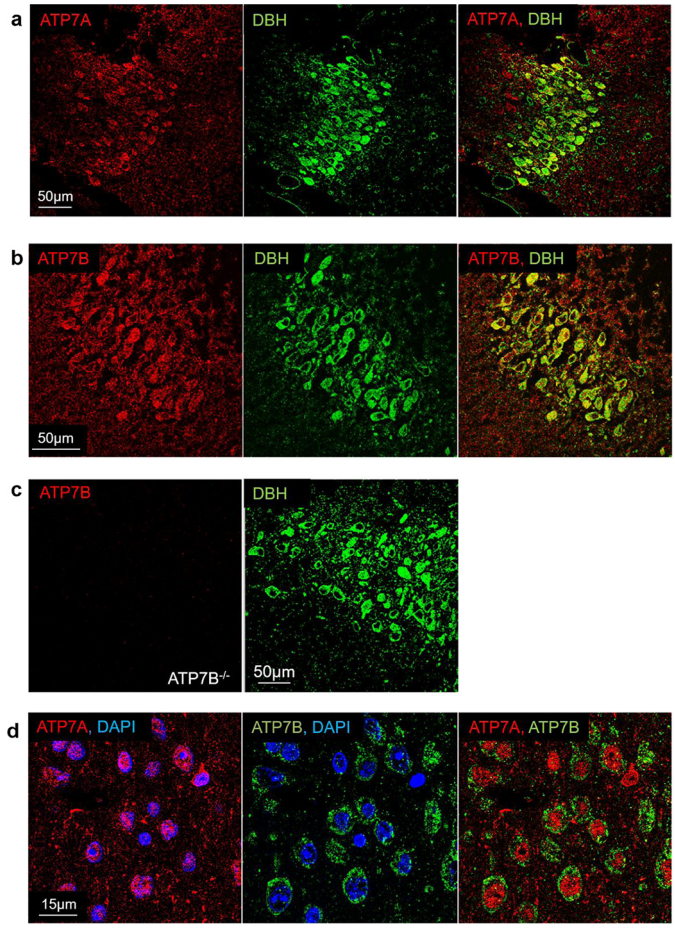

Figure 3. Expression and localization of ATP7A and ATP7B in neurons of LC. *a* and *b*, co-immunostaining of ATP7A (*a*) or ATP7B (*b*) shown in *red* with DBH (in *green*) illustrates the presence of ATP7A and ATP7B in neurons expressing DBH (*yellow*). *c*, specificity of anti-ATP7B antibody is confirmed by the lack of staining in sections from *Atp7b*$^{-/-}$ mice, the LC in these sections is identified by DBH expression, as elsewhere. *d*, high-magnification image of DBH-expressing neurons shows distinct intracellular localization of ATP7A (*red*) and ATP7B (*green*). *Left*, ATP7A is clustered asymmetrically in the vicinity of the nuclei, identified by DAPI staining (*blue*). *Middle*, ATP7B is vesicular and distributed throughout the cytosol. *Right*, co-localization of ATP7A and ATP7B shows no overlap between the patterns.

Down-regulation of ATP7A or ATP7B has opposite effects on DBH export from SH-SY5Y cells

DBH has a complex intracellular behavior, which includes proteolytic processing, sorting within the secretory pathway, and export. To determine whether any of these steps depend on the activity of ATP7A and/or ATP7B, we individually decreased ATP7A and ATP7B levels in SH-SY5Y cells using siRNA (Fig. 5*a*). The maximum down-regulation using nucleofection was ~50% for either ATP7A or ATP7B (Fig. 5*b*). Down-regulation of ATP7A did not cause a compensatory up-regulation of ATP7B (a slight decrease in protein intensity was observed), and reciprocally, down-regulation of ATP7B did not significantly alter the ATP7A levels (Fig. 5*b*). This lack of significant changes in the abundance of one Cu-ATPase in response to down-regulation of the other is consistent with a previously reported lack of such compensatory changes in a brain (28).

The DBH protein levels showed a trend toward being higher upon down-regulation of either ATP7A or ATP7B (1.21 ± 0.14, $n = 3$, $p = 0.2$; and 1.50 ± 0.19, $n = 3$, $p = 0.054$, respectively), but the increase was not statistically significant. The most notable effect was on the abundance of extracellular DBH under resting conditions (constitutive secretion), which was significantly and oppositely affected by the ATP7A and ATP7B knockdowns (Fig. 5*d*). The down-regulation of ATP7A decreased the amount of DBH in the growth medium by 20% (0.81 ± 0.06, $p = 0.0265$) compared with cells treated with a nontargeting siRNA, whereas ATP7B knockdown increased the extracellular levels of DBH by 53% (1.53 ± 0.13, $p = 0.004$) (Fig. 5*c*). To better characterize the relationship between the two Cu transporters and DBH export, we correlated the remaining cellular levels of ATP7A or ATP7B after siRNA treatment with the amount of extracellular DBH (Fig. 5*d*). The levels of ATP7A in cells positively correlated with the amount of exported DBH (Fig. 5*d*, *upper panel*), *i.e.* ATP7A facilitates the export of DBH. In contrast, the protein levels of ATP7B showed negative correlation with the secreted DBH (Fig. 5*d*, *lower panel*), *i.e.* ATP7B was inhibitory to DBH secretion.

The activity of DBH in the extracellular medium remained proportional to DBH protein, independently of which Cu transporter was inhibited (Fig. 5*e*). Specifically, ATP7A down-regulation decreased the total DBH activity in the medium by 23% (0.28 ± 0.01 *versus* 0.36 ± 0.04, $p = 0.116$), whereas ATP7B knockdown increased the DBH activity in the medium by ~60% (0.58 ± 0.02 *versus* 0.36 ± 0.04, $p = 0.002$). Normalizing DBH activity to DBH protein confirmed that the specific activity of extracellular DBH was largely unaffected by either ATP7A or ATP7B knockdowns (93 ± 4% of control for ATP7A knockdown and 105 ± 3% of control for ATP7B knockdown) (Fig. 5*f*). This result suggests that DBH is exported from cells in an active Cu-bound form and that DBH activation and export could be coupled. The significant increase in total DBH activity, with no change in DBH activity/protein (Fig. 5*g*), strongly suggests that ATP7B negatively regulates the abundance of extracellular DBH (rather than its enzymatic activity), which is a novel function for this transporter.

ATP7A and ATP7B do not co-localize with DBH in the post-Golgi compartments

The role of either ATP7A or ATP7B in regulating protein secretion has not been reported previously. To better understand how ATP7A and ATP7B can influence the export of soluble DBH, we first determined whether under basal conditions ATP7A and/or ATP7B were targeted to DBH-containing vesicles or secretory granules. For the purpose of this study, we defined secretory granules as DBH-positive compartments with an average diameter of 0.45–1.12 μm and intense DBH staining. The smaller, more heterogeneous compartments with a less intense DBH staining were defined as vesicles. Our co-immunostaining experiments illustrate that ATP7A does not co-localize with DBH in either vesicles or granules (Fig. 6*a*, *left panels*). This result was not surprising because ATP7A is targeted primarily to the TGN (as expected). ATP7B and DBH both show vesicular localization; however, these vesicles are distinct, *i.e.* ATP7B is not targeted to DBH-positive vesicles/granules (Fig. 6*a*, *right panels*). The lack of co-localization between DBH and ATP7B was also observed in primary neu-

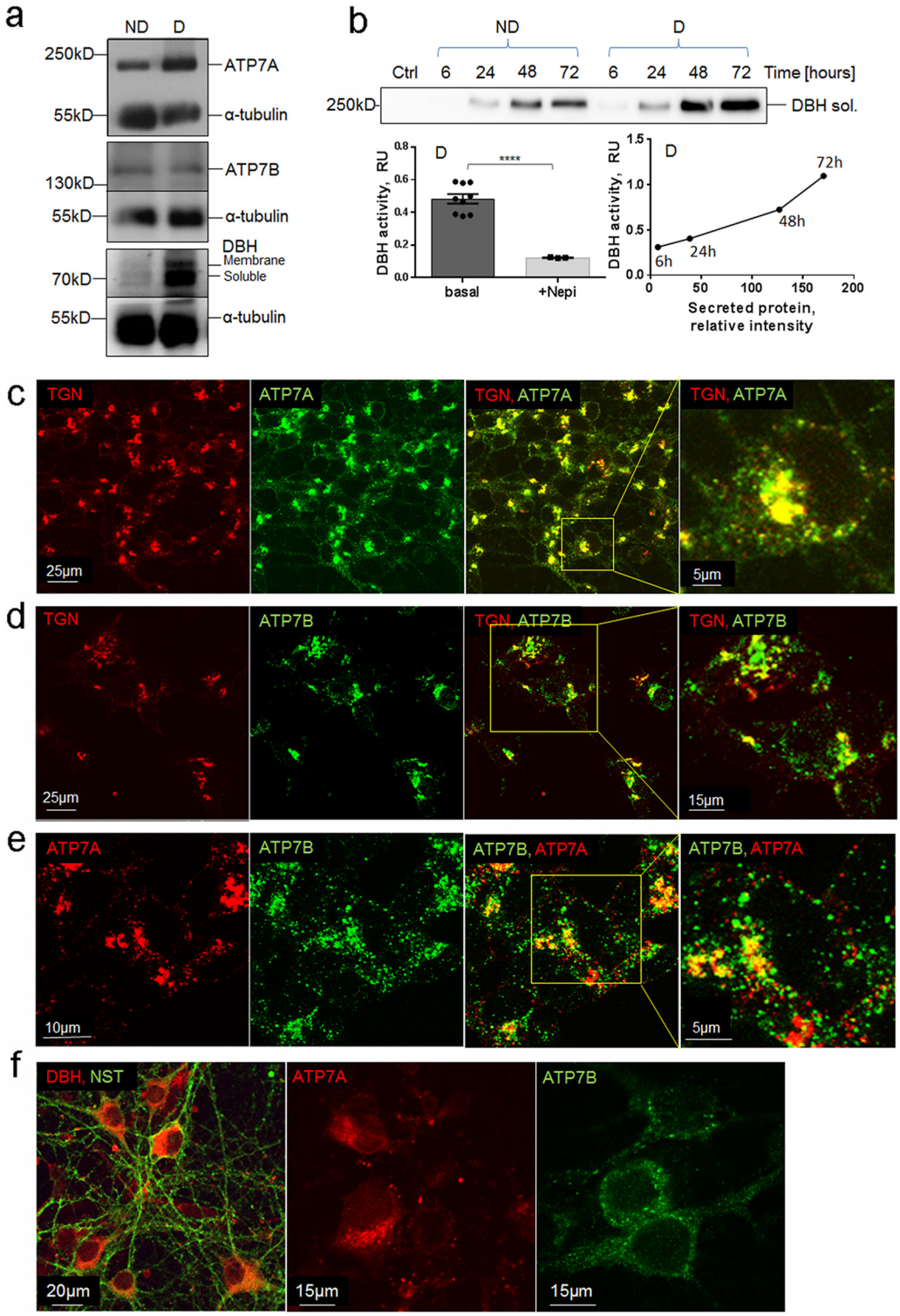

Figure 4. SH-SY5Y as a model system to study the relationship between Cu and DBH. *a*, representative Western blotting demonstrates expression of ATP7A, ATP7B, and DBH in nondifferentiated (*ND*) and differentiated (*D*) SH-SY5Y cells. Staining with α-tubulin is used as a loading control. *b*, *top*, constitutive secretion of DBH is time-dependent and is higher in differentiated cells. *Bottom left*, extracellular DBH is active. The specificity of the assay was confirmed using the DBH inhibitor nepicastat (*Nepi*), which inhibited 75% of the signal (0.48 ± 0.03, $n = 9$, *versus* 0.12 ± 0.01, $n = 3$; $p < 0.001$). *Bottom right*, the amount of DBH protein and DBH activity in the extracellular medium increases over time. *c*, in differentiated SH-SY5Y cells, ATP7A (*green*) is targeted mostly to the TGN (*red*). Co-localization of ATP7A and TGN (*yellow*) also shows a smaller fraction of ATP7A in vesicles. *d*, in basal conditions, ATP7B (*green*) is targeted mostly to vesicles with a smaller fraction overlapping with the TGN (*red*). *e*, co-localization of ATP7A (*red*) and ATP7B (*green*) shows a partial overlap in the TGN (*yellow*) and no overlap in vesicles. ATP7A is localized to small vesicles that are distinct from ATP7B-positive large vesicles. *f*, *left*, primary cortical neurons visualized by immunostaining for neurospecific β3-tubulin (*green*) express DBH (*red*). *Middle* and *right*, ATP7A (*red*) and ATP7B (*green*) are present in cortical primary neurons and show distinct localization pattern. ATP7A staining is perinuclear and asymmetric, whereas ATP7B is distributed more uniformly in vesicles. In *panels c–e*, the regions in *boxes* are enlarged at the adjacent panel.

rons (Fig. 6*b*). Taken together, these data demonstrate that neither ATP7A nor ATP7B is present at detectable levels in the DBH-positive post-Golgi compartments. Therefore, they regulate vesicular DBH indirectly, most likely by influencing Cu levels in cells. The loading of the DBH catalytic site with Cu, which likely takes place when DBH traffics through the TGN on its way to vesicles/granules, may contribute to the regulation of DBH cellular distribution.

ATP7B-dependent decrease of Cu in the cytosol inhibits DBH export

At this point, our data could be rationalized by the following model. In noradrenergic neurons, ATP7A is targeted to the TGN and transfers Cu to DBH when a newly synthesized DBH traffics through the TGN to its final destinations. ATP7B functions in vesicles to sequester excess Cu away from ATP7A and inhibits excessive DBH secretion. To test the predicted role of ATP7B in limiting Cu access to ATP7A, we overexpressed ATP7B in SH-SY5Y cells and primary cortical neurons using adenovirus-mediated infection (Fig. 7*a*). Changes in cytosolic Cu were evaluated by measuring the mRNA levels for the copper chaperone CCS, which are responsive to cytosolic Cu levels and are higher when Cu is low, at least in some tissues (29, 30).

Upon ATP7B overexpression, the abundance of CCS mRNA increased 2-fold, consistent with a decrease in cytosolic Cu (Fig. 7*b*). The levels of ATP7A were unchanged (Fig. 7*c*). Under these conditions, the amounts of intracellular DBH increased (Fig. 7*d*) and extracellular DBH decreased significantly (Fig. 7*e*). Thus, the excess ATP7B limits Cu levels in the cytosol, and this deficiency inhibits DBH export. To verify that the inhibition of constitutive DBH secretion was related to ATP7B activity and not merely protein overexpression, we measured the levels of extracellular DBH following expression of a catalytically inactive mutant of ATP7B, ATP7B-D1027A (Fig. 7*f*). This inactive mutant was expressed at higher levels than the WT ATP7B but produced no change in DBH secretion (Fig. 7*f*). We confirmed these findings in the primary cortical neurons (Fig. 7*g*). Overexpression of ATP7B in these neurons showed an increase in intracellular DBH (Fig. 7*g*), whereas extracellular DBH was markedly decreased (Fig. 7*h*). Inhibition of DBH export was not observed when neurons expressed an inactive ATP7B-D1027A mutant. These results confirm that the activity of ATP7B is responsible for the regulation of DBH export.

Cu is required for constitutive export of DBH

The down-regulation of ATP7A is expected to increase Cu levels in the cytosol (at least temporarily), whereas overexpression of ATP7B decreases cytosolic Cu; yet both manipulations inhibit DBH export. It is possible that either high or low cytosolic Cu inhibits DBH export. More likely, the inhibition of DBH secretion is a result of insufficient Cu availability in the lumen of the TGN (which would occur upon either ATP7A down-regulation or ATP7B overexpression). To test more directly whether low and/or high Cu influence constitutive secretion of DBH, we treated the SH-SY5Y cells for 5 and 16 h with either excess Cu or a combination of an extracellular Cu chelator, bathocuproine disulfonate (BCS), and an intracellular Cu chelator, tetrathiomolybdate (TTM), to decrease Cu levels (Fig. 8, *a* and *b*).

Excess Cu within a physiological range of concentrations did not significantly alter the levels of extracellular DBH (Fig. 8*b*). In contrast, Cu limitation significantly inhibited DBH export, and the effect was stronger with a longer chelation time. Depleting Cu for 16 h increased DBH in cells by ~5-fold compared with nontreated cells (Fig. 8*a*). Concomitantly, DBH concentration in the medium was decreased by 43% (Fig. 8*b*). Thus, we concluded that Cu is required for constitutive export of DBH.

Cu depletion does not inhibit DBH proteolytic processing but modifies the pattern of DBH-positive compartments

DBH retention in cells upon Cu depletion could be caused by the inhibition of proteolytic processing within the secretory pathway. However, analysis of the proteolytic pattern of DBH under low and high Cu (as well as following the knockdowns of the Cu transporters) revealed that neither condition blocked the proteolytic conversion of membrane-bound DBH (Fig. 8*a*). With a prolonged Cu chelation, the shorter variant of DBH was not only produced but was more abundant. Consequently, to better understand how Cu deficiency affects DBH export, we examined the targeting of DBH to intracellular compartments in more detail.

Under basal conditions, the sizes of DBH-containing compartments vary significantly (Fig. 8*c*, *left panels*), but the intensity of DBH staining is stronger in larger compartments with a median area close to 0.025 mm^2, which is consistent with the size of secretory granules (31). Cu limitation does not cause retention of DBH in the TGN (the fraction of DBH in the TGN increases only marginally (by 8.5%)). Instead, we observed a significant change in the sizes of DBH-positive compartments: the average diameter of these compartments was 37% smaller in the Cu-depleted cells compared with nontreated cells (Fig. 8*c*, *right panels*, and Fig. 8*d*). Thus, Cu limitation affects the post-Golgi DBH-positive compartments. The observed morphologic changes are consistent with inhibition of vesicle maturation and/or fusion.

Discussion

The roles of mammalian ATP7A and ATP7B in Cu delivery to Cu-dependent enzymes within the secretory pathway and maintenance of Cu homeostasis in tissues are well-established. In this study, we have described a new and previously unappreciated role for ATP7A and ATP7B in the regulation of extracellular levels of active DBH. This finding adds to a growing list of the Cu-dependent regulatory processes in the brain. Changes in Cu levels have been shown to influence the activity and trafficking of Cu transporters (32–34), modulate a kinase-mediated phosphorylation (35–37), regulate mRNA abundance (38), and modulate neuronal activity (3, 4, 6, 39). Our current data suggest that changes in Cu availability may also alter the intracellular sorting and/or secretion of soluble DBH in the absence of neuronal stimuli. The extracellular DBH is enzymatically active; therefore, changes in the abundance of DBH in the extracellular milieu may upset the existing balance of DA and/or NE. Future studies in animal models are needed to directly test this hypothesis, which is intriguing because it may explain the

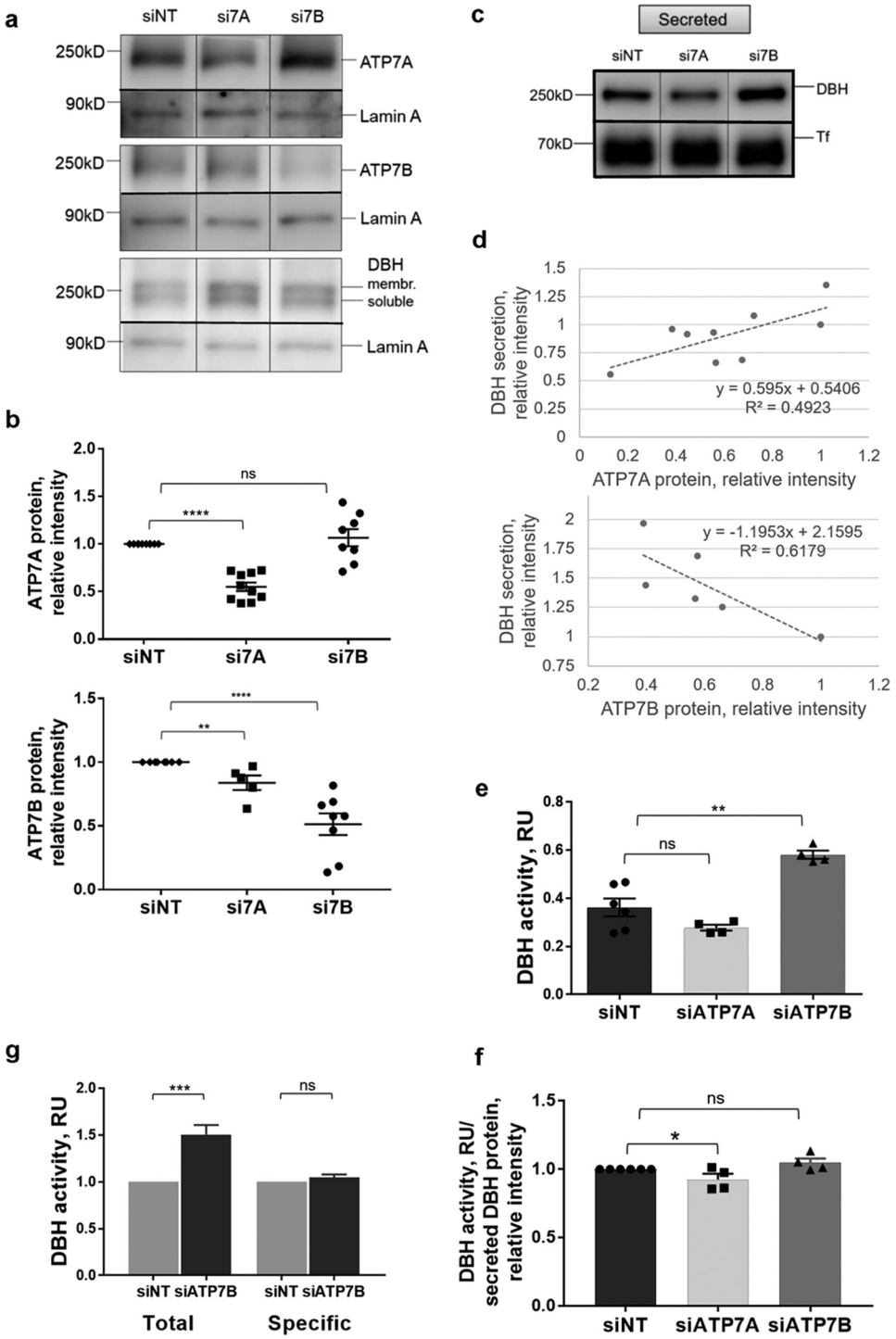

Figure 5. Cu-ATPases play opposite roles in DBH secretion and activity. *a*, Western blotting illustrating protein levels following siRNA-mediated down-regulation of ATP7A (*si7A*) or ATP7B (*si7B*). A nontargeting siRNA (*siNT*) was used as a control. *b*, densitometry data. *Top*, ATP7A was decreased on average by 45% (0.55 ± 0.05, $n = 10$; $p < 0.001$) following transfection with si7A, whereas si7B had little effect on ATP7A abundance. *Bottom*, ATP7B abundance was decreased on average by 49% (0.51 ± 0.09, $n = 8$; $p < 0.001$) upon transfection with si7B; transfection with si7A caused only a slight decrease (0.84 ± 0.06, $n = 5–8$; $p = 0.038$; data normalized to the siNT controls) *c*, DBH abundance in the medium is decreased upon ATP7A down-regulation and increased upon ATP7B down-regulation. The medium was collected 48 h post-nucleofection. *d*, the levels of ATP7A protein in cells correlate positively with the amount of extracellular DBH, whereas ATP7B levels correlate negatively with extracellular DBH. *e*, an equal amount of the growth medium from the same number of cells was used to measure DBH activity (*RU* (relative units) is absorbance at 330 nm). The down-regulation of ATP7A decreases the activity of DBH compared with control (0.28 ± 0.01 and 0.36 ± 0.04, respectively, $n = 4–6$; $p = 0.12$). The ATP7B knockdown results in a higher DBH activity in the cell medium compared with control (0.58 ± 0.02 and 0.36 ± 0.04, respectively, $n = 4–6$; $p < 0.001$). *f*, specific activity of extracellular DBH (DBH activity/DBH protein) is unchanged upon down-regulation of ATP7A (0.93 ± 0.04, $n = 4$; $p = 0.049$) or ATP7B (1.05 ± 0.03, $n = 4$; $p = 0.08$) when compared with control taken as 1. *g*, total DBH activity in the cell medium increases upon ATP7B down-regulation ($n = 6$; $p < 0.001$), whereas specific activity of DBH is unchanged ($n = 4$; $p = 0.17$), consistent with an increased abundance of active DBH protein.

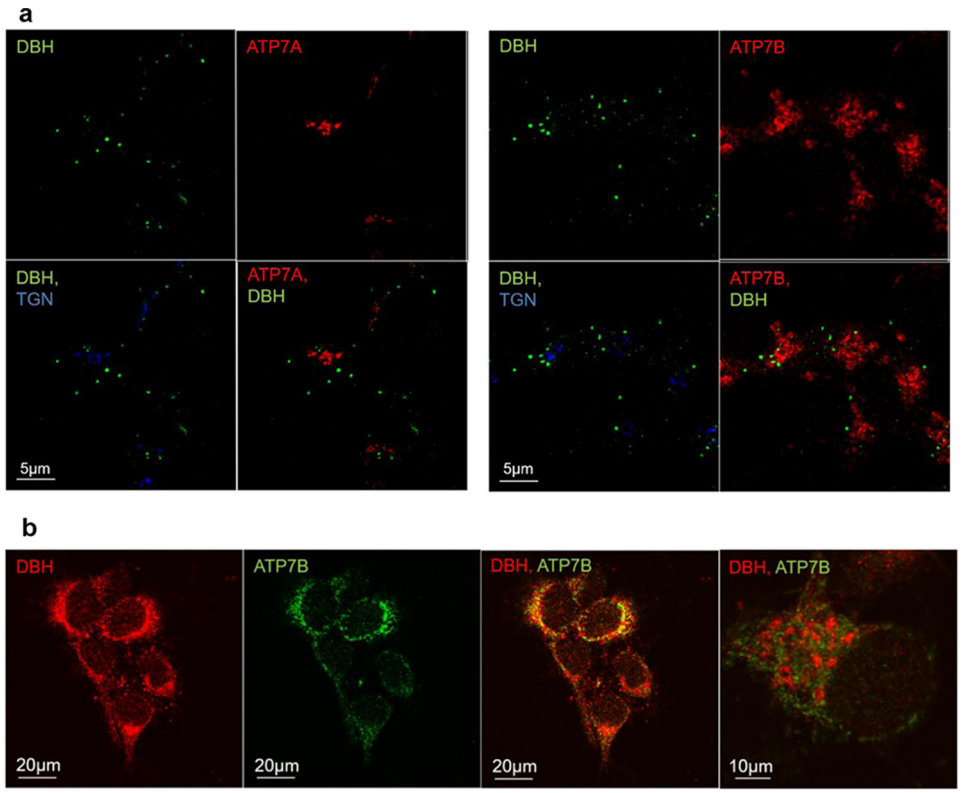

Figure 6. Cu-ATPases are not targeted to DBH-positive cell compartments. *a*, *left*, co-staining for ATP7A (*red*), TGN (*blue*), and DBH (*green*) in differentiated SH-SY5Y cells. *Right*, Co-staining for ATP7B (*red*), TGN (*blue*), and DBH (*green*). DBH does not overlap with the TGN marker. Neither ATP7A nor ATP7B shows targeting to the DBH-positive compartments. *b*, immunostaining of DBH (*red*) and ATP7B (*green*) in hippocampal neurons. Although the low-magnification image suggests an overlap (*yellow*), the high-magnification view of the "overlap" area (*right*) clearly shows distinct localization of ATP7B and DBH.

reported impact of ATP7B inactivation on the dopaminergic system in Wilson disease patients and animals.

Our results allow for several other predictions. In Parkinson's disease, low Cu is reported in DBH-expressing neurons (40, 41). Our data suggest that Cu depletion would be inhibitory to both NE production and DA clearance. These defects cannot be alleviated by treatment with L-dihydroxyphenylalanine (L-DOPA) even if DBH expression is not compromised, because Cu is required for the enzymatic activity of DBH. Similarly, in neurologic Wilson disease, excessive Cu chelation may cause local Cu deficiency in such Cu-requiring neurons as the neurons of LC and shift the catecholamine levels and/or ratio. Catecholamine misbalance may explain the worsening neurologic symptoms and psychotic episodes commonly observed in Wilson disease patients on Cu chelation therapy (42).

Thus far, the functional significance of ATP7A and ATP7B co-expression in the brain has not been very clear. Our studies provide direct evidence that two Cu transporters, ATP7A and ATP7B, have distinct and nonoverlapping functions in DBH-expressing neurons. The literature (12), as well as our finding that ATP7A does not co-localize with DBH in secretory granules *in vitro* and *in vivo*, strongly suggests that ATP7A transfers Cu to DBH when it transitions through the TGN. ATP7B localization in distinct vesicles and the effects of overexpression point to the role of ATP7B in sequestering Cu for storage in vesicles. The distinct localization of Cu transporters and the apparent competition for Cu enable opposite regulation of DBH. The observed changes in DBH abundance are consistent with the regulation of DBH export, although at present we cannot formally rule out the potential effects of ATP7A/7B down-regulation on DBH protein stability and/or slight changes in total protein expression.

We found that a mild increase of Cu supply to neuronal cells does not affect DBH secretion, whereas down-regulation of ATP7B, which increases the amount of Cu available to ATP7A, stimulates secretion. These results may appear contradictory, but they could be explained by sequestration of excess Cu (added extracellularly) by ATP7B, a process that is lost when ATP7B is down-regulated.

ATP7A and ATP7B are structurally similar. It is thought that both Cu transporters receive their Cu from the cytosolic copper chaperone Atox1 through direct protein–protein interactions. Previous studies using solution NMR have uncovered differences between ATP7A and ATP7B in their interactions with the Cu–Atox1 complex (43, 44). However, it remains unclear whether these structural differences translate into a measurable preference of Cu–Atox1 toward ATP7A or ATP7B. Atox1 is highly expressed in LC (23), and these high levels may be sufficient to accommodate the function of both transporters, although this possibility needs to be tested directly. It is also possible that the distribution of Cu between ATP7A and ATP7B is governed by the relative abundance of each transporter in cells. In either scenario, changes in the abundance of one of the Cu transporters would make more Cu available to the other. This may alter their transport activity and localization, further altering Cu distribution in cells, and disregulate Cu-dependent enzymes. In other words, to better understand

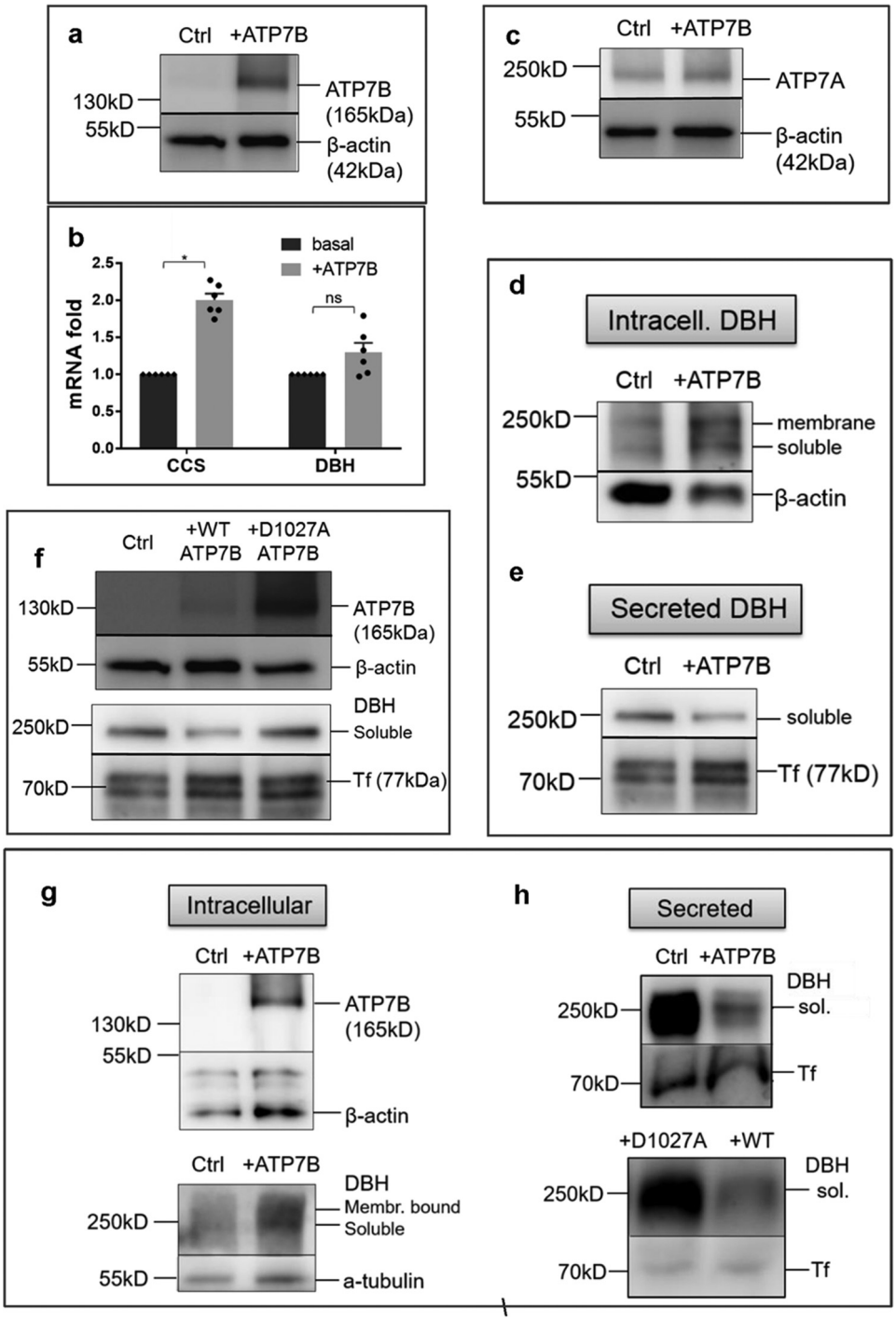

Figure 7. Overexpression of ATP7B inhibits DBH secretion by lowering Cu in the cytosol. *a*, ATP7B was overexpressed in SH-SY5Y cells using adenovirus; the endogenous ATP7B in nontransfected controls was barely detectable at the same exposure time. *b*, ATP7B overexpression is associated with an increase in the CCS mRNA abundance (2.0 ± 0.085-fold, $n = 3$; $p < 0.001$) suggestive of the decrease in the cytosolic Cu. DBH mRNA was unchanged (1.3 ± 0.13-fold; $p = 0.42$). *c*, ATP7B overexpression does not affect ATP7A abundance. *d* and *e*, upon ATP7B overexpression, both soluble and membrane-bound DBH accumulate in cells (*d*), whereas DBH in the medium is markedly decreased (*e*). *f*, *top*, a catalytically inactive of ATP7B variant (D1027A) is highly expressed compared with WT ATP7B. *Bottom*, despite higher expression, the D1027A mutant does not decrease the levels of extracellular DBH. *g*, overexpression of ATP7B in primary cortical neurons (*top*) is associated with an increased retention of DBH in cells (actin and tubulin are loading controls). *h*, *top*, overexpression of WT ATP7B in cortical neurons decreases DBH secretion compared with control. The levels of DBH exported from cells expressing a catalytically inactive D1027A mutant are much higher than from cells expressing the WT ATP7B.

the neurologic Wilson disease (which is mechanistically less clear than the Menkes disease phenotype), future studies in animals should take into account a spectrum of consequences of ATP7B inactivation.

The requirement for Cu homeostasis in DBH activity and secretion implies that the brain regions innervated by DBH-expressing neurons can be sensitive to Cu misbalance, and the consequences of Cu misbalance may differ depending on Cu

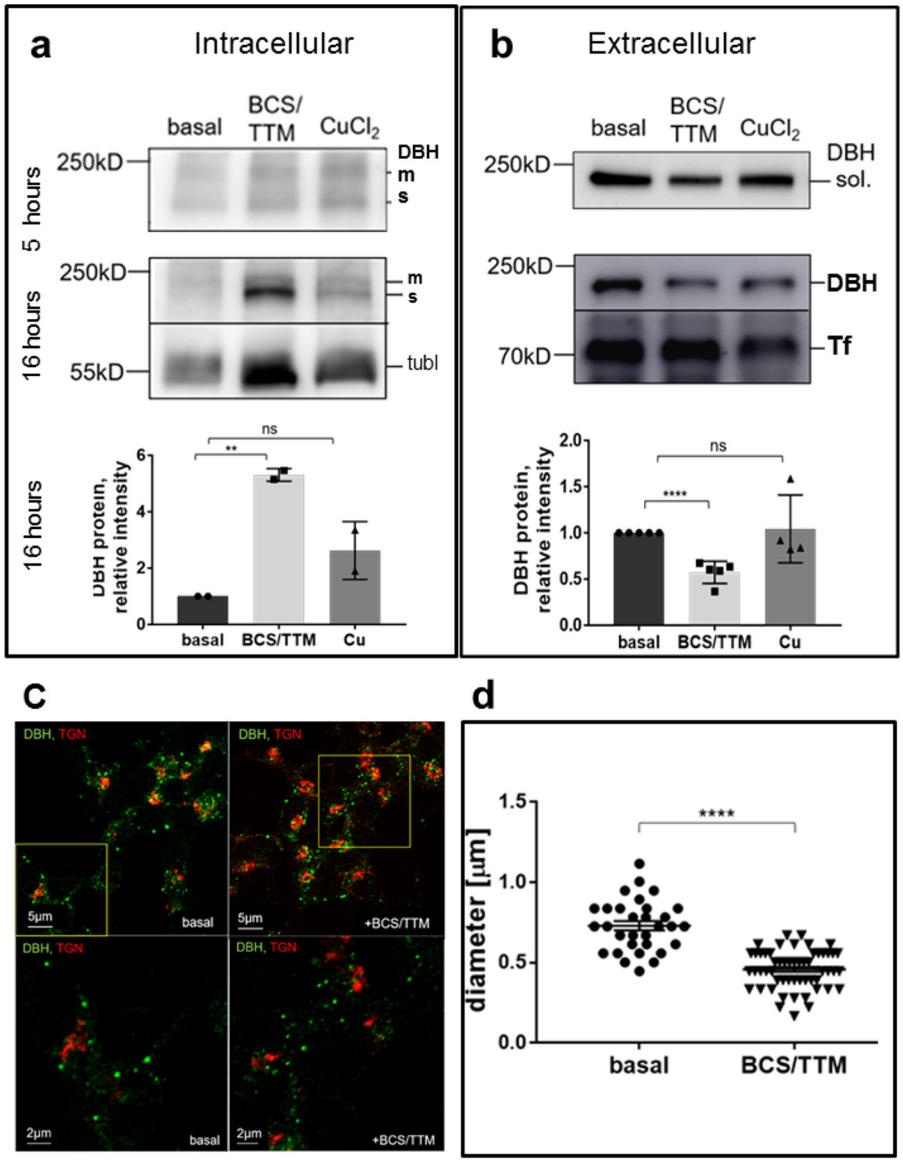

Figure 8. Copper is required for constitutive secretion of DBH. *a* and *b*, SH-SY5Y cells were treated with 10 μM $CuCl_2$ or 10 μM Cu chelators (BCS/TTM) added to the culture medium for 5 and 16 h. Cells in the basal medium served as a control. *a*, retention of DBH in cells increases upon Cu chelation, especially after 16 h (5.3 $\pm$ 0.16-fold increase, $n = 3$; $p = 0.001$). The addition of Cu does not significantly change DBH retention (0.86 $\pm$ 0.06, $n = 3$; $p = 0.13$). Representative Western blotting is shown. The *bar graphs* represent the densitometry data. The intensities of individual bands were normalized to those of tubulin (*tubl*), which was used as a loading control, and compared with values at basal conditions. *b*, the extracellular levels of DBH decrease in response to Cu chelation, especially after a prolonged treatment (0.57 $\pm$ 0.05-fold, $n = 5$; $p < 0.001$). Excess Cu does not significantly alter DBH secretion (1.0 $\pm$ 0.18-fold, $n = 4$; $p = 0.80$). *Upper panels*, Western blotting. *Lower panel*, densitometry data for the 16-h time point. The intensities of individual bands were normalized to transferin (*Tf*), used as a loading control and compared with values under basal conditions. *m*, membrane; *s*, soluble. *c*, co-staining of DBH (*green*) and TGN (*red*) under basal (*left panels*) and Cu-chelated conditions (*right panels*). *Upper panels* show lower magnification; areas outlined by *yellow squares* are magnified and shown in the *lower panels*. *d*, the diameter of DBH-positive compartments was assessed using the Fiji software line tool. Cu depletion with BCS/TTM is associated with the decrease in the size of DBH-positive compartments compared with those in the basal conditions (0.46 μm $\pm$ 0.02, $n = 55$, and 0.73 μm $\pm$ 0.03, $n = 31$, respectively; $p < 0.001$).

levels. Previous studies revealed a complex pattern of changes in Cu levels in the brains of ATP7B-deficient Long-Evans Cinnamon (LEC) rats. These rats show a Cu deficiency in the brain early in the disease (at 4 and 10 weeks) and a low NE/DA ratio (46). As Cu levels in the brain increase, the levels of both catecholamines normalize (in 20-week-old rats). Such time-dependent changes in the Cu and catecholamine levels in response to ATP7B inactivation could be relevant to the variability in the time of onset and magnitude of neuropsychiatric symptoms in Wilson disease patients (47–49).

In conclusion, we have provided new evidence for the functional significance of Cu in brain physiology, shed light on the mechanisms that integrate Cu and catecholamine metabolism, and identified the Cu transport machinery that regulate the export of soluble DBH from noradrenergic neurons. These findings open new avenues for studies on the role of Cu misbalance in neuropsychiatric disorders.

Materials and methods

Immunohistochemistry of brain slices

Mice were housed at the Johns Hopkins University (JHU) animal care facility with food and water provided *ad libitum*. The described studies were approved by the JHU Animal Care

and Use Committee. For tissue sectioning, mice were perfused with 30 ml of PBS followed by 30 ml of 4% paraformaldehyde (PFA), which was kept at 4 °C. The brains were incubated overnight in 4% PFA at 4 °C and then transferred to 30% sucrose in PBS and incubated for 48–72 h at 4 °C until the brains sank to the bottom of the tube. The brains were cut coronally to remove the frontal third, and the rest was embedded in optimum tissue cutting compound (OCT) (with the cutting site to the bottom of a cubical cryomold). Blocks were frozen at −80 °C for at least 24 h. Starting from the cerebellum, the brains were first trimmed using 100-μm slices to approach the brainstem. The sections containing LC were then obtained by cutting six 30-μm-thick slices. The slices were placed into a 24-well plate, washed three times with PBS (each wash for 5 min), and permeabilized for 24 h with 0.5% Triton-X in PBS (PBST). The slices were washed with PBST (three times for 5 min each), and a primary antibody was added for 18 h at a 1:500 dilution in PBST. The slices were then washed with PBST (three washes for 10 min each), and a secondary antibody was diluted at 1:1000 in PBST with DAPI (1 μg/ml) were added for 16 h. The 24-well plate was wrapped in aluminum foil and incubated at 4 °C overnight. Subsequently, the slices were washed with PBST (three times for 5 min each) and then washed in PBS for 5 min. The slices were transferred with a pencil brush into a water container and then mounted on positively charged glass slides. Sections were cover-slipped with the mounting medium (Fluoromount without DAPI) and imaged using confocal microscopy.

X-ray fluorescence microscopy (XFM)

For metal imaging, the brains sections were prepared as described above, and then every other section was stained with anti-DBH antibodies (for identification of LC). The adjacent sections were placed on Ultralene® film, glued to the aluminum sample holders, and then fastened to a plexiglass mount inside the hutch for metal analysis by XFM. The XFM data were collected on a beamline 8-BM at the Advanced Photon Source, Argonne National Laboratory (Argonne, IL). The incident X-ray energy was tuned to 10 keV using a Si-monochromator, and the monochromatic beam was focused to 35 × 35 μm using a Kirkpatrick-Baez mirror (Advanced Photon Source). The samples were placed at 45° to the incident X-ray beam, and the resulting X-ray fluorescence was collected at 90° using an energy-dispersive four-element detector (Vortex ME-4, SII Nanotechnology, Northridge, CA). Raster scanning of the entire section was done in a fly-scan mode with 35 × 35–μm steps (500 ms/point).

The two-dimensional maps for each element were generated following the background subtraction and fitting each element's fluorescence photon counts using MAPS software (50). The fluorescence counts were translated into $\mu g/cm^2$ using calibrated X-ray standards (AXO, Dresden, Germany). Metal concentrations in the regions of interest were converted into volume concentrations using 30-μm tissue thickness with the assumption that the X-ray beam fully penetrated the sample. For Cu, the volume concentrations were further divided by the molecular weight of Cu (63.55 mg/mmol) to obtain mM concentrations.

SH-SY5Y cell culture

All experiments with SH-SY5Y cells, except those shown in Fig. 4, *a* and *b*, were done with fully differentiated cells. Experiments with the siRNA-mediated down-regulation of ATP7A and ATP7B were done in cells differentiated in the presence of retinoic acid (see below). The standard differentiation protocol was as follows. The SH-SY5Y cells were cultured in complete medium (MEM/F12 mixture, 1:1), supplemented with 10% fetal bovine serum and 1% penicillin/streptomycin. Cells were plated at ~20% confluence and differentiated over a period of 7 days. Culture was treated twice with 10 μM retinoic acid in complete medium for 2 days each time followed by 50 nM brain-derived neurotrophic factor for 3 days in serum-free MEM/F12 medium (26).

For various treatments, fresh serum-free medium was added to differentiated SH-SY5Y cells cultured in 6-cm dishes, and cells were incubated for 5 h with one of the following reagents: 10 μM BCS, 10 μM TTM, or 10 μM $CuCl_2$. Cells grown in a medium without additions were used as a control. Following incubations, the cells were homogenized in RIPA buffer (Millipore 20-188) and centrifuged for 10 min at 3000 × *g*. Prior to homogenization, the medium was collected, concentrated on a 30-kDa cutoff concentrator (Vivaspin 6, GE Healthcare) by centrifugation for 15 min at 4000 × *g*, and used for SDS-PAGE and a DBH activity assay. The protein concentration in the cell pellets and the medium was determined by BCA assay.

Western blotting

Proteins (30–50 μg) in 2× loading buffer (1 M Tris-HCl, pH 6.8, 10% SDS, glycerol, 1% β-mercaptoethanol, and 1% bromphenol blue) were separated by 8% Laemmli SDS-PAGE. Following separation, proteins were transferred to polyvinylidene difluoride membrane using the CAPS buffer with 10% methanol. Membranes were blocked for 1 h at room temperature in 3% BSA/PBS, washed with PBS, and incubated overnight with the primary antibody dissolved in 2% BSA/PBS. Primary antibodies were anti-ATP7A (Santa Cruz Biotechnology sc-376467), anti-ATP7B (Abcam ab124973), and anti-DBH (Cell Signaling Technology 8586). Membranes were washed with PBST and PBS and blotted with the secondary antibodies conjugated to Alexa Fluor series 488 or 555 for 2 h in 2% BSA/PBS. Following another washing with PBST and PBS, membranes were exposed to ECL 10:1 pico:femto mix (Thermo Fisher Scientific 34095) and imaged using chemiluminescence.

Immunostaining of SH-SY5Y cells

SH-SY5Y cells were grown on collagen-coated coverslips in 12-well plates. For collagen coating, sterilized coverslips were incubated with sterile collagen dissolved in 1% acetic acid in H_2O. Ammonium hydroxide was added onto the lid of 12-well plates to allow for reaction with collagen and precipitation on the surface of coverslips. After 20 min, ammonium hydroxide and the collagen solution were aspirated, and wells were washed twice with 2 ml of sterile PBS. Plates were dried for at least 1 h in a sterile hood. SH-SY5Y cells were plated at ~20% confluence and differentiated as described above. Following differentiation, cells were washed with PBS and fixed with 4%

PFA/PBS for 15 min at room temperature. Cells were then washed twice with PBS and permeabilized with 0.2% Triton X-100 in PBS.

For immunostaining, the fixed and permeabilized cells were washed twice with PBS and blocked with 1% gelatin, 1% BSA in PBS. The primary antibodies, ATP7A (Santa Cruz Biotechnology sc-376467), ATP7B (in-house N-WND), and DBH (Dr. Eipper, University of Connecticut) were diluted at 1:250 in 1% gelatin, 1% BSA in PBS. Coverslips with attached cells were placed on Parafilm, 75 μl of the primary antibody solution was added per coverslip, and cells were incubated for 2 h. The coverslips were placed back into the 12-well plate and washed twice in PBST and once with PBS. Coverslips were placed on a new Parafilm and incubated for 1 h with the secondary antibody conjugated with Alexa Fluor series 488 or 555. The secondary antibodies were used at a 1:500 dilution and complemented with 1:1000 DAPI. Coverslips were dipped in H_20 for 10 s and mounted with Fluoromount (Thermo Fisher Scientific 00-4958-02) on glass slides. Slides were imaged using a Zeiss 500 confocal microscope with Zen software and a 63× or 100× lens. An LSM image browser was used to import images and obtain image information.

Enzymatic activity of DBH

DBH activity was measured as described previously (51). In this assay, the surrogate substrate of DBH, tyramine, is converted by DBH to octopamine, an intermediate product. The mixture is applied to a protonated Dowex ion-exchange resin packed into mini-columns. The eluted octopamine is then oxidized by sodium periodate to *para*-hydroxybenzaldehyde, which is quantified spectrophotometrically by absorbance at 330 nm. The ion-exchange Dowex slurry (50:50 slurry, Dowex: water) was protonated as following. The slurry was mixed with 1 M NaOH in a glass beaker and poured onto the filter paper. The Dowex resin was first washed with 1 M NaOH and then with deionized water until neutral pH eluate was measured (standard pH paper). Dowex resin was then washed with 1 M HCl and then with water until the eluate was at neutral pH. Dowex resin (0.4 ml) was packed into a Bio-Rad Micro-Spin^{TM} column and washed twice with 2 ml of H_2O.

A typical reaction mix (for 24 samples) contained 6 ml of sodium acetate, pH 5, 1.5 ml of 0.2 M fumarate, 1.5 ml of 0.2 M ascorbate, 1.5 ml of 0.02 mM pargyline, 4.5 ml of 0.2 M *N*-ethylmaleimide, 3 ml of catalase, and 6 ml of H_2O. Once prepared, 0.8 ml of the above mix was pipetted into plastic centrifuge tubes, and 50 μl of cell medium (concentrated as described above) was added. To initiate the reaction, 100 μl of tyramine was added and mixed by vortexing. Samples were incubated for 0.5 h at 37 °C, and the reaction was stopped by adding 0.2 ml of 20% perchloric acid and vortexing. Tyramine was added to buffer blanks following this step. Samples were centrifuged for 20 min at 5000 rpm or 12,000 × *g* for 5–10 min to pellet the protein precipitate. Supernatant was placed on Microspin Dowex columns, and the octopamine product was eluted into glass test tubes with 4 N NH_4OH (1 ml twice). To the eluate, 0.2 ml of 2% $NaIO_4$ mix was added, and after 6 min, 0.2 ml of 10% $Na_2S_20_5$ was added to stop the reaction. Absorbance at 330 nm was measured at room temperature.

Down-regulation of ATP7A and ATP7B in SH-SY5Y cells using siRNA

SH-SY5Y cells were transfected with siRNA for ATP7A or ATP7B (SMARTpool, Dharmacon), and nontargeting siRNA was used as a control. The Amaxa nucleofection system and Nucleofector Kit V were used, with cells prepared as described previously (52). Specifically, 2 × 10^5/cm^2 cells were plated/sample, and cell pellet was resuspended in 100 μl of Nucleofector® solution/sample. 300 nM siRNA was added, and samples were loaded into a cuvette, which was then placed into the Amaxa system. Nucleofection was done using a "high viability" setting (A023).

The transfected cells were incubated for 48 h before medium was collected, and cells were pelleted with RIPA buffer. Total protein concentration was determined with BCA analysis. Western blot analysis showed that the nucleofection protocol yielded ~50% down-regulation of either of the Cu-ATPases, which was higher and more reproducible than transfection with Lipofectamine. Additionally, the cell medium was harvested, and protein concentration was determined for Western blot analysis of DBH.

Primary neurons

Cortical neurons were isolated from E17.5 mice as described previously (53). Neurons were plated in Neurobasal-A medium supplemented with B-27, glutamine, and penicillin/streptomycin. The primary cell culture was transfected with GFP for the identification of neurons and subsequently immunostained with antibodies against ATP7A (Santa Cruz Biotechnology sc-376467), ATP7B (Abcam ab124973/in-house N-WND), and DBH (a generous gift from Dr. Eipper) followed by conjugating the secondary antibodies to Alexa Fluor series 488 or 555. From a separate batch, primary cortical neurons were plated in a 10-cm dish for Western blot analysis of DBH protein. Growth medium from plated primary neurons was collected and passed through a 30-kDa cutoff column for concentration of DBH and subsequent measurements of DBH activity.

Adenoviral transfection of ATP7B into SH-SY5Y cells/cortical primary neurons

Adenoviral construct pS3106 with the coding region for the full-length WT ATP7B, and the ATP7B D1027A mutant were prepared as described previously (45). The viruses with ATP7B (3.2 × 10^{12} viral particles/ml) or D1027A (2 × 10^8 viral particles/ml) were used to transfect SH-SY5Y cells or primary cortical neurons (prepared as described above) in 10-cm dish at a 1:1000 dilution. Cells were incubated with either virus for 2 h at 37 °C and then washed. Neurons were subsequently incubated for 18 h to allow for new protein synthesis. Cells were harvested using RIPA buffer (Millipore 20-188), and protein concentration was determined by BCA assay. Western blotting was performed for ATP7B and DBH using 30 μg of cell lysate protein. Additionally, the culture medium was collected and run through a 30-kDa cutoff column, protein concentration was determined, and 30 μg of concentrate was analyzed by SDS-PAGE and Western blotting gel to detect secreted DBH.

Statistical analysis

Statistical analysis was performed using GraphPad Prism software. An unpaired *t* test was applied, and significance was determined based on the *p* value (differences with a *p* value <0.05 were considered significant).

Data availability

All representative data in support of the conclusions are included with this article. The complete set of data can be provided upon request to the authors.

Author contributions—K. S., T. S., and S. L. data curation; K. S. and T. S. formal analysis; K. S. and M. R. validation; K. S., M. R., S. J., and A. M. investigation; K. S., M. R., T. S., B. B., and A. M. methodology; K. S. writing-original draft; M. R., T. S., B. B., and S. L. writing-review and editing; S. L. conceptualization; S. L. funding acquisition; S. L. project administration.

Acknowledgments—Hippocampal neurons were provided by Dr. Kirill Gorshkov. Use of the Advanced Photon Source at Argonne National Laboratory was supported by the U. S. Department of Energy, Office of Science, Office of Basic Energy Sciences, under contract DE-AC02-06CH11357. We thank Evan Maxey and Dr. Stefan Vogt for user support and assistance at the Advanced Photon Source. We thank Dr. Betty Eipper for expert advice and the kind gift of the antibody. We thank members of the Lutsenko laboratory for critical reading of the manuscript and helpful comments.

References

1. Scheiber, I. F., Mercer, J. F., and Dringen, R. (2014) Metabolism and functions of copper in brain. *Prog. Neurobiol.* **116,** 33–57 CrossRef Medline
2. Cunnane, S. C., and Crawford, M. A. (2014) Energetic and nutritional constraints on infant brain development: Implications for brain expansion during human evolution. *J. Hum. Evol.* **77,** 88–98 CrossRef Medline
3. Dodani, S. C., Firl, A., Chan, J., Nam, C. I., Aron, A. T., Onak, C. S., Ramos-Torres, K. M., Paek, J., Webster, C. M., Feller, M. B., and Chang, C. J. (2014) Copper is an endogenous modulator of neural circuit spontaneous activity. *Proc. Natl. Acad. Sci. U.S.A.* **111,** 16280–16285 CrossRef Medline
4. Schlief, M. L., Craig, A. M., and Gitlin, J. D. (2005) NMDA receptor activation mediates copper homeostasis in hippocampal neurons. *J. Neurosci.* **25,** 239–246 CrossRef Medline
5. Gaier, E. D., Miller, M. B., Ralle, M., Aryal, D., Wetsel, W. C., Mains, R. E., and Eipper, B. A. (2013) Peptidylglycine α-amidating monooxygenase heterozygosity alters brain copper handling with region specificity. *J. Neurochem.* **127,** 605–619 CrossRef Medline
6. Gaier, E. D., Eipper, B. A., and Mains, R. E. (2013) Copper signaling in the mammalian nervous system: Synaptic effects. *J. Neurosci. Res.* **91,** 2–19 Medline
7. Gaier, E. D., Rodriguiz, R. M., Zhou, J., Ralle, M., Wetsel, W. C., Eipper, B. A., and Mains, R. E. (2014) *In vivo* and *in vitro* analyses of amygdalar function reveal a role for copper. *J. Neurophysiol.* **111,** 1927–1939 CrossRef Medline
8. Salazar-Weber, N. L., and Smith, J. P. (2011) Copper Inhibits NMDA receptor-independent LTP and modulates the paired-pulse ratio after LTP in mouse hippocampal slices. *Int. J. Alzheimers Dis.* **2011,** 864753 Medline
9. Goldstein, D. S., Holmes, C. S., and Kaler, S. G. (2009) Relative efficiencies of plasma catechol levels and ratios for neonatal diagnosis of Menkes disease. *Neurochem. Res.* **34,** 1464–1468 CrossRef Medline
10. Kaler, S. G., Gahl, W. A., Berry, S. A., Holmes, C. S., and Goldstein, D. S. (1993) Predictive value of plasma catecholamine levels in neonatal detection of Menkes disease. *J. Inherit. Metab. Dis.* **16,** 907–908 CrossRef Medline
11. Kaler, S. G., Goldstein, D. S., Holmes, C., Salerno, J. A., and Gahl, W. A. (1993) Plasma and cerebrospinal fluid neurochemical pattern in Menkes disease. *Ann. Neurol.* **33,** 171–175 CrossRef Medline
12. Kaler, S. G., and Holmes, C. S. (2013) Catecholamine metabolites affected by the copper-dependent enzyme dopamine-β-hydroxylase provide sensitive biomarkers for early diagnosis of Menkes disease and viral-mediated ATP7A gene therapy. *Adv. Pharmacol.* **68,** 223–233 CrossRef Medline
13. Barthel, H., Sorger, D., Kühn, H. J., Wagner, A., Kluge, R., and Hermann, W. (2001) Differential alteration of the nigrostriatal dopaminergic system in Wilson's disease investigated with [123I]β-CIT and high-resolution SPET. *Eur. J. Nucl. Med.* **28,** 1656–1663 CrossRefMedline
14. Mangold, J. B., and Klinman, J. P. (1984) Mechanism-based inactivation of dopamine β-monooxygenase by β-chlorophenethylamine. *J. Biol. Chem.* **259,** 7772–7779 Medline
15. Ash, D. E., Papadopoulos, N. J., Colombo, G., and Villafranca, J. J. (1984) Kinetic and spectroscopic studies of the interaction of copper with dopamine β-hydroxylase. *J. Biol. Chem.* **259,** 3395–3398 Medline
16. Xiao, T., Ackerman, C. M., Carroll, E. C., Jia, S., Hoagland, A., Chan, J., Thai, B., Liu, C. S., Isacoff, E. Y., and Chang, C. J. (2018) Copper regulates rest-activity cycles through the locus coeruleus-norepinephrine system. *Nat. Chem. Biol.* **14,** 655–663 CrossRef Medline
17. Qian, Y., Tiffany-Castiglioni, E., and Harris, E. D. (1997) A Menkes P-type ATPase involved in copper homeostasis in the central nervous system of the rat. *Brain Res. Mol. Brain Res.* **48,** 60–66 CrossRef Medline
18. Gerbasi, V., Lutsenko, S., and Lewis, E. J. (2003) A mutation in the ATP7B copper transporter causes reduced dopamine β-hydroxylase and norepinephrine in mouse adrenal. *Neurochem. Res.* **28,** 867–873 CrossRef Medline
19. Sabban, E. L., Greene, L. A., and Goldstein, M. (1983) Mechanism of biosynthesis of soluble and membrane-bound forms of dopamine β-hydroxylase in PC12 pheochromocytoma cells. *J. Biol. Chem.* **258,** 7812–7818 Medline
20. Saxena, A., and Fleming, P. J. (1983) Isolation and reconstitution of the membrane-bound form of dopamine β-hydroxylase. *J. Biol. Chem.* **258,** 4147–4152 Medline
21. Oyarce, A. M., and Fleming, P. J. (1991) Multiple forms of human dopamine β-hydroxylase in SH-SY5Y neuroblastoma cells. *Arch. Biochem. Biophys.* **290,** 503–510 CrossRef Medline
22. O'Connor, D. T., Cervenka, J. H., Stone, R. A., Levine, G. L., Parmer, R. J., Franco-Bourland, R. E., Madrazo, I., Langlais, P. J., Robertson, D., and Biaggioni, I. (1994) Dopamine β-hydroxylase immunoreactivity in human cerebrospinal fluid: Properties, relationship to central noradrenergic neuronal activity and variation in Parkinson's disease and congenital dopamine β-hydroxylase deficiency. *Clin. Sci.* (*Lond.*) **86,** 149–158 Medline
23. Naeve, G. S., Vana, A. M., Eggold, J. R., Kelner, G. S., Maki, R., Desouza, E. B., and Foster, A. C. (1999) Expression profile of the copper homeostasis gene, *rAtox1*, in the rat brain. *Neuroscience* **93,** 1179–1187 CrossRef Medline
24. Popescu, B. F., and Nichol, H. (2011) Mapping brain metals to evaluate therapies for neurodegenerative disease. *CNS Neurosci. Ther.* **17,** 256–268 CrossRef Medline
25. Nishihara, E., Furuyama, T., Yamashita, S., and Mori, N. (1998) Expression of copper trafficking genes in the mouse brain. *Neuroreport* **9,** 3259–3263 CrossRef Medline
26. Kovalevich, J., and Langford, D. (2013) Considerations for the use of SH-SY5Y neuroblastoma cells in neurobiology. *Methods Mol. Biol.* **1078,** 9–21 CrossRef Medline
27. Hatori, Y., Yan, Y., Schmidt, K., Furukawa, E., Hasan, N. M., Yang, N., Liu, C. N., Sockanathan, S., and Lutsenko, S. (2016) Neuronal differentiation is associated with a redox-regulated increase of copper flow to the secretory pathway. *Nat. Commun.* **7,** 10640 CrossRef Medline
28. Niciu, M. J., Ma, X. M., El Meskini, R., Pachter, J. S., Mains, R. E., and Eipper, B. A. (2007) Altered ATP7A expression and other compensatory responses in a murine model of Menkes disease. *Neurobiol. Dis.* **27,** 278–291 CrossRef Medline
29. Fu, S., Jiang, W., and Zheng, W. (2015) Age-dependent increase of brain copper levels and expressions of copper regulatory proteins in the subventricular zone and choroid plexus. *Front Mol. Neurosci.* **8,** 22 Medline

30. Han, H., Archibeque, S. L., and Engle, T. E. (2009) Characterization and identification of hepatic mRNA related to copper metabolism and homeostasis in cattle. *Biol. Trace Elem. Res.* **129,** 130–136 CrossRef Medline
31. Hendy, G. N., Li, T., Girard, M., Feldstein, R. C., Mulay, S., Desjardins, R., Day, R., Karaplis, A. C., Tremblay, M. L., and Canaff, L. (2006) Targeted ablation of the chromogranin a (*Chga*) gene: Normal neuroendocrine dense-core secretory granules and increased expression of other granins. *Mol. Endocrinol.* **20,** 1935–1947 CrossRef Medline
32. Veldhuis, N. A., Valova, V. A., Gaeth, A. P., Palstra, N., Hannan, K. M., Michell, B. J., Kelly, L. E., Jennings, I., Kemp, B. E., Pearson, R. B., Robinson, P. J., and Camakaris, J. (2009) Phosphorylation regulates copper-responsive trafficking of the Menkes copper transporting P-type ATPase. *Int. J. Biochem. Cell Biol.* **41,** 2403–2412 CrossRef Medline
33. Hasan, N. M., Gupta, A., Polishchuk, E., Yu, C. H., Polishchuk, R., Dmitriev, O. Y., and Lutsenko, S. (2012) Molecular events initiating exit of a copper-transporting ATPase ATP7B from the trans-Golgi network. *J. Biol. Chem.* **287,** 36041–36050 CrossRef Medline
34. Braiterman, L., Nyasae, L., Leves, F., and Hubbard, A. L. (2011) Critical roles for the COOH terminus of the Cu-ATPase ATP7B in protein stability, trans-Golgi network retention, copper sensing, and retrograde trafficking. *Am. J. Physiol. Gastrointest. Liver Physiol.* **301,** G69–G81 CrossRef Medline
35. Bartee, M. Y., Ralle, M., and Lutsenko, S. (2009) The loop connecting metal-binding domains 3 and 4 of ATP7B is a target of a kinase-mediated phosphorylation. *Biochemistry* **48,** 5573–5581 CrossRef Medline
36. Pilankatta, R., Lewis, D., and Inesi, G. (2011) Involvement of protein kinase D in expression and trafficking of ATP7B (copper ATPase). *J. Biol. Chem.* **286,** 7389–7396 CrossRef Medline
37. Gupta, A., Bhattacharjee, A., Dmitriev, O. Y., Nokhrin, S., Braiterman, L., Hubbard, A. L., and Lutsenko, S. (2011) Cellular copper levels determine the phenotype of the Arg875 variant of ATP7B/Wilson disease protein. *Proc. Natl. Acad. Sci. U.S.A.* **108,** 5390–5395 CrossRef Medline
38. Gao, C., Zhu, L., Zhu, F., Sun, J., and Zhu, Z. (2014) Effects of different sources of copper on Ctr1, ATP7A, ATP7B, MT and DMT1 protein and gene expression in Caco-2 cells. *J. Trace Elem. Med. Biol.* **28,** 344–350 CrossRef Medline
39. Doreulee, N., Yanovsky, Y., and Haas, H. L. (1997) Suppression of long-term potentiation in hippocampal slices by copper. *Hippocampus* **7,** 666–669 CrossRef Medline
40. Davies, K. M., Bohic, S., Carmona, A., Ortega, R., Cottam, V., Hare, D. J., Finberg, J. P., Reyes, S., Halliday, G. M., Mercer, J. F., and Double, K. L. (2014) Copper pathology in vulnerable brain regions in Parkinson's disease. *Neurobiol. Aging* **35,** 858–866 CrossRef Medline
41. Zecca, L., Stroppolo, A., Gatti, A., Tampellini, D., Toscani, M., Gallorini, M., Giaveri, G., Arosio, P., Santambrogio, P., Fariello, R. G., Karatekin, E., Kleinman, M. H., Turro, N., Hornykiewicz, O., and Zucca, F. A. (2004) The role of iron and copper molecules in the neuronal vulnerability of locus coeruleus and substantia nigra during aging. *Proc. Natl. Acad. Sci. U.S.A.* **101,** 9843–9848 CrossRef Medline
42. Zhang, J. W., Liu, J. X., Hou, H. M., Chen, D. B., Feng, L., Wu, C., Wei, L. T., and Li, X. H. (2015) Effects of tetrathiomolybdate and penicillamine on brain hydroxyl radical and free copper levels: A microdialysis study *in vivo*. *Biochem. Biophys. Res. Commun.* **458,** 82–85 CrossRef Medline
43. Banci, L., Bertini, I., Cantini, F., Chasapis, C. T., Hadjiliadis, N., and Rosato, A. (2005) A NMR study of the interaction of a three-domain construct of ATP7A with copper(I) and copper(I)-HAH1: The interplay of domains. *J. Biol. Chem.* **280,** 38259–38263 CrossRef Medline
44. Banci, L., Bertini, I., Cantini, F., Massagni, C., Migliardi, M., and Rosato, A. (2009) An NMR study of the interaction of the N-terminal cytoplasmic tail of the Wilson disease protein with copper(I)-HAH1. *J. Biol. Chem.* **284,** 9354–9360 CrossRef Medline
45. Jayakanthan, S., Braiterman, L. T., Hasan, N. M., Unger, V. M., and Lutsenko, S. (2017) Human copper transporter ATP7B (Wilson disease protein) forms stable dimers *in vitro* and in cells. *J. Biol. Chem.* **292,** 18760–18774 CrossRef Medline
46. Saito, T., Nagao, T., Okabe, M., and Saito, K. (1996) Neurochemical and histochemical evidence for an abnormal catecholamine metabolism in the cerebral cortex of the Long-Evans Cinnamon rat before excessive copper accumulation in the brain. *Neurosci. Lett.* **216,** 195–198 CrossRef Medline
47. Woerwag-Mehta, S., Hindley, P., Hedderly, T., and Dhawan, A. (2011) Complex psychiatric presentation in adolescent onset Wilson's disease. *BMJ Case Rep.* **2011,** bcr0120102628 CrossRef Medline
48. Hegde, S., Sinha, S., Rao, S. L., Taly, A. B., and Vasudev, M. K. (2010) Cognitive profile and structural findings in Wilson's disease: A neuropsychological and MRI-based study. *Neurol. India* **58,** 708–713 CrossRef Medline
49. Benhamla, T., Tirouche, Y. D., Abaoub-Germain, A., and Theodore, F. (2007) The onset of psychiatric disorders and Wilson's disease. *Encephale* **33,** 924–932 CrossRef Medline
50. Vogt, S. (2003) MAPS: A set of software tools for analysis and visualization of 3D X-ray fluorescence data sets. *J. Phys. IV France* **104,** 635–638 CrossRef
51. Nagatsu, T., and Udenfriend, S. (1972) Photometric assay of dopamine-3-hydroxylase activity in human blood. *Clin. Chem.* **18,** 980–983 Medline
52. Slanina, H., Schmutzler, M., Christodoulides, M., Kim, K. S., and Schubert-Unkmeir, A. (2012) Effective plasmid DNA and small interfering RNA delivery to diseased human brain microvascular endothelial cells. *J. Mol. Microbiol. Biotechnol.* **22,** 245–257 CrossRef Medline
53. Tolias, K. F., Bikoff, J. B., Burette, A., Paradis, S., Harrar, D., Tavazoie, S., Weinberg, R. J., and Greenberg, M. E. (2005) The Rac1-GEF Tiam1 couples the NMDA receptor to the activity-dependent development of dendritic arbors and spines. *Neuron* **45,** 525–538 CrossRef Medline